PHYSICAL REVIEW RESEARCH 1, 012005(R) (2019)

Rapid Communications

Ultrafast transient increase of oxygen octahedral rotations in a perovskite

M. Porer,[1,*] M. Fechner,[2] M. Kubli,[3] M. J. Neugebauer,[3] S. Parchenko,[1] V. Esposito,[4] A. Narayan,[5] N. A. Spaldin,[5] R. Huber,[6] M. Radovic,[1] E. M. Bothschafter,[1] J. M. Glownia,[7] T. Sato,[7] S. Song,[7] S. L. Johnson,[3,4] and U. Staub[1,†]

[1]*Swiss Light Source, Paul Scherrer Institute, 5232 Villigen-PSI, Switzerland*
[2]*Max Planck Institute for the Structure and Dynamics of Matter, CFEL, 22761 Hamburg, Germany*
[3]*Institute for Quantum Electronics, ETH Zürich, 8093 Zürich, Switzerland*
[4]*SwissFEL, Paul Scherrer Institute, 5232 Villigen-PSI, Switzerland*
[5]*Materials Theory, ETH Zürich, 8093 Zürich, Switzerland*
[6]*Department of Physics, University of Regensburg, 93040 Regensburg, Germany*
[7]*LCLS, SLAC National Accelerator Laboratory, Menlo Park, California 94025, USA*

(Received 14 February 2019; published 9 August 2019)

We present femtosecond hard x-ray diffraction experiments that study the effect of photodoping on the perovskite $EuTiO_3$. We observe an ultrafast transient increase of reflection intensities that are directly related to the antiferrodistortive rotation of the oxygen octahedra. This increase relates directly to an increase of the order parameter associated with a purely structural phase transition that is opposite to the behavior of increasing the materials temperature. First-principles calculations show that the creation of electron-hole pairs leads to changes in the vibrational potential that is consistent with an increase of the order parameter. The order parameter increase can be understood from an ultrafast charge-transfer-induced reduction of the Goldschmidt tolerance factor, which is a fundamental control parameter for the properties of perovskites.

DOI: 10.1103/PhysRevResearch.1.012005

Phase transitions are commonly described by an order parameter (OP) that represents the degree of order in the system. Within the ordered phase, the OP quantifies the amplitude of an ordering phenomenon or the distance to the critical point with respect to a tuning parameter such as temperature, structural parameters, or the electronic chemical potential. Examples of OPs include the amplitude of a symmetry-breaking distortion of a crystal structure and the amount of charge carriers in a charge/orbital-density wave or a superconducting condensate. In correlated materials, structural or electronic ordering phenomena often occur simultaneously or compete with each other [1]. Slight changes in a tuning parameter can induce a phase transition with potentially useful functionality.

Optical control of such tuning parameters [2] opens up the possibility to manipulate an OP and thereby control possibly connected macroscopic material properties on ultrafast timescales. In many materials where the ultrafast control of crystalline structures has been explored, optical excitation pushes materials towards their less ordered high-temperature phase [3–10] as electronically driven ordered phases melt and possible concomitant structural modifications relax. Novel routes to optically *increase* an OP have been explored recently with the goal of enhancing or inducing functional properties. Examples include light-enhanced superconductivity [10,11], light-induced ferromagnetism [12], and increased charge- [13] or spin- [14] density-wave amplitudes. A significant potential exists for increasing an order parameter by coherently controlling the structural parameters [15–18].

Second-order purely structural phase transitions are driven by anharmonic interactions within the phonon system [19,20]. When a tuning parameter reaches the critical point, the structure spontaneously distorts along a vibrational coordinate which lowers the symmetry of the crystal. The corresponding OP is the mean displacement amplitude [20]. At the critical point of a displacive [20] structural transition, the eigenfrequency of the respective vibrational mode, called the soft mode, approaches zero and the susceptibility of the OP with respect to the tuning parameter diverges.

$EuTiO_3$ is a cubic perovskite ($Pm\bar{3}m$) at high temperature which undergoes a structural phase transition around $T \approx 290$ K driven by an acoustic soft mode at the R point which manifests as an antiferrodistortive (AFD) rotation of the oxygen octahedra [Fig. 1(a)], very similar to that in $SrTiO_3$ [21–23]. The rotation angle φ is the order parameter of the transition [20]. Here, we photoexcite $EuTiO_3$ in its low-temperature structurally distorted phase ($I4/mcm$) via ultrafast optical excitation across its direct band gap of 0.9 eV [24]. Via subsequent femtosecond hard x-ray pulses we monitor the intensities of AFD-induced x-ray superlattice (SL) reflections [Fig. 1(b)] which are proportional to φ^2 [9].

$EuTiO_3$ films were grown by pulsed laser deposition (PLD) at the PLD facility of the Surface/Interface Spectroscopy (SIS, X09LA) beamline at the Swiss Light Source (SLS), Paul Scherrer Institute. The films were deposited on commercial $SrTiO_3$ (001) substrates (purchased from SurfaceNet

*science@porer.org
†Urs.Staub@psi.ch

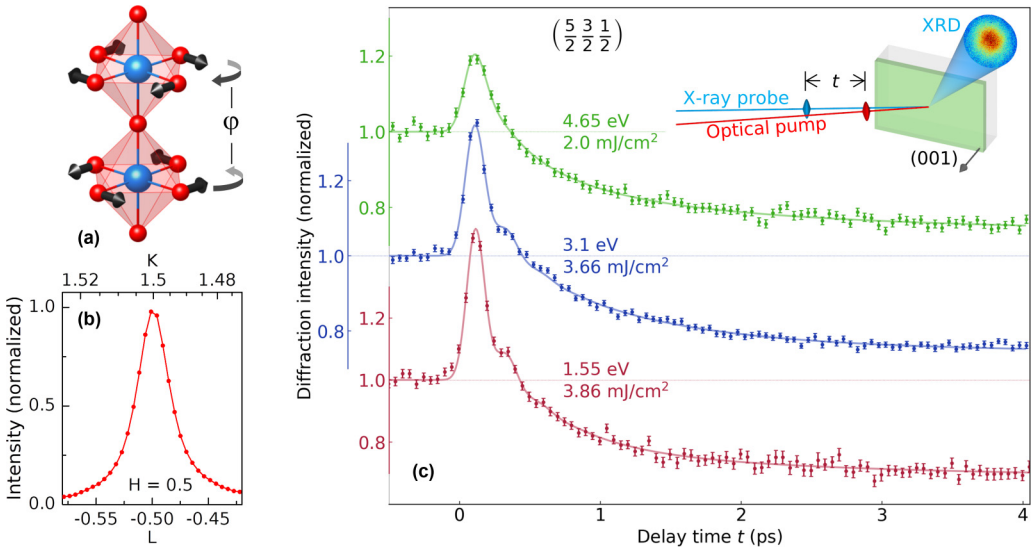

FIG. 1. (a) Ti (blue) and O (red) atoms of two cubic unit cells stacked along the c axis. Arrows indicate atomic motions of the oxygen sites during the AFD transition and the direction of the octahedral rotation angle φ. (b) Equilibrium rocking curve of a typical superlattice reflection of the 40-nm thin $EuTiO_3$ film measured at $T = 120$ K. (c) Dynamics of the $(\frac{5}{2}\frac{3}{2}\frac{1}{2})$ superlattice reflection intensity upon photoexcitation at $T = 120$ K. The labels denote the pump photon energy and the absorbed excitation fluence. The blue and red solid lines result from a fit of the phenomenological model explained in the text and the Supplemental Material [25]. The green solid line is a guide to the eye. Inset: Schematic of the femtosecond x-ray diffraction (XRD) experiment.

GmbH) in a very low oxygen partial pressure of 10^{-7} mbar (base pressure of the PLD chamber 10^{-9} mbar) and at a temperature of 750 °C. The phase transition of the 40-nm film was characterized using static x-ray diffraction [Fig. 1(b) and Supplemental Material (SM) Fig. S1 [25]]. Compared to $EuTiO_3$ ceramic material [22], we find the critical temperature to be elevated to $T_c \approx 650$ K, which we attribute to oxygen defects [22] and/or residual strain [26].

For time-resolved x-ray diffraction experiments, we photoexcite the $EuTiO_3$ thin film with 50-fs-long pulses derived either from the fundamental ($\langle E_p \rangle = 1.55$ eV), the second harmonic ($\langle E_p \rangle = 3.1$ eV), or the third harmonic ($\langle E_p \rangle = 4.65$ eV) of a Ti:sapphire amplifier system. We estimate the absorbed fluence in the film via an optical transfer matrix formalism [27] based on the the optical constants of $EuTiO_3$ and the $SrTiO_3$ substrate (SM [25]). The injected densities of e-h pairs for the laser harmonics are 6×10^{-2}, 3×10^{-2}, and 2×10^{-2} per formula unit (f.u.) and 1 mJ/cm^2 absorbed fluence of 1.55, 3.1, and 4.65 eV excitation energies, respectively. Approximately 50-fs-long x-ray pulses with 9.5 keV photon energy delivered by Linac Coherent Light Source (LCLS) (SLAC) were used to probe the SL reflection intensity after excitation (SM [25]). The sample was cooled with a N_2 cryoblower to $T = 120$ K to remain above the critical temperature for the AFD transition of the $SrTiO_3$ substrate at $T = 105$ K [23]. Supplementary optical pump-probe studies were performed at the FEMTO-facility at Swiss Light Source using 80-fs-long pulses with a central photon energy of 1.55 eV. Additional time-resolved optical-pump/multi-THz probe studies were performed at the University of Regensburg [25]. The density functional theory (DFT) computations are carried out utilizing the all-electron full-potential linearized augmented plane-wave implementation within the ELK code [28]. As an approximation for the exchange-correlation functional we apply a generalized gradient approach plus U (GGA+U) and apply a $U = 6.2$ eV and $J = 1$ eV, respectively, on the Eu $4f$ states. The muffin tin radii for Eu, Ti, and O are set to 1.3, 0.9, and 0.75 Å. We used a basis set of $l_{\max_{APW}} = 10$, an $8 \times 8 \times 6$ k-point sampling of the Brillouin zone, and took the product of the average muffin tin radius and the maximum reciprocal lattice vector to be 8.5. Further numerical parameters are adjusted to the high-quality (highq.true.) settings within the ELK code.

Figure 1(c) shows the normalized intensity of the $(\frac{5}{2}\frac{3}{2}\frac{1}{2})$ SL reflection as a function of the pump-probe delay for a series of excitation conditions. The green/blue/red data points show the transient SL intensity obtained for excitation with photon energies of 4.65/3.1/1.55 eV for an absorbed fluence of 2.0/3.66/3.86 mJ/cm^2 injecting a density of 0.04/0.11/0.23 electron-hole (e-h) pairs per formula unit (f.u.), respectively. Independent of the pump photon energies and fluences/injected carrier densities, we observe a transient increase of the superlattice diffraction intensity (I_{AFD}) within an initial sub-ps time window. The enhancement is similar for another AFD-induced SL reflection with different x-ray momentum transfer (SM Fig. S2 [25]). Quantitatively, the maximum observed enhancement factor of I_{AFD} is 1.4 for the highest injected density with 1.55 eV photons. The subsequent decay of I_{AFD} intersects the initial baseline. For excitation with photon energies below 4.65 eV the decay exhibits a superimposed strongly damped oscillatory component with a frequency of approximately 4 THz. Furthermore, when lowering the excitation intensity we find that the decay slows down and the lifetime of the enhanced diffraction intensity increases (Fig. 2). The base temperature does not significantly influence the dynamics (SM Fig. S3 [25]). As I_{AFD} scales with φ^2, the enhanced diffraction efficiency may originate from an increase of the OP.

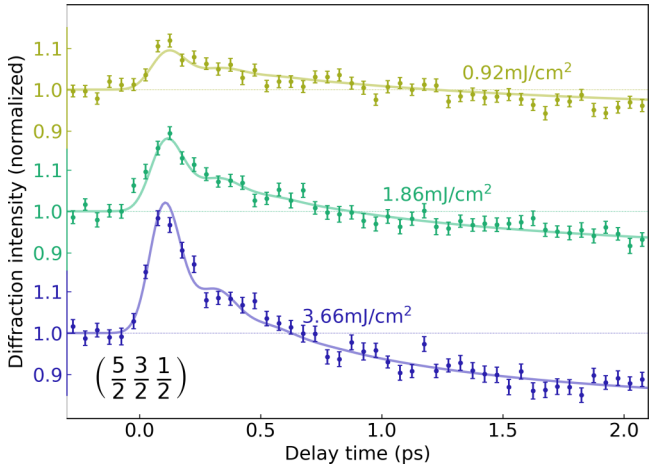

FIG. 2. Transient superlattice diffraction intensity for a series of excitation fluences. The pump photon energy is set to 3.1 eV and the temperature is 120 K. The solid lines are derived from a numerical fit to the model described in the text.

To describe this behavior we calculate the total energy within the $I4/mcm$ unit cell at a series of fixed rotation angles (SM Fig. S4 [25]) and from there we derive the double-well potential of the AFD mode (SM [25]). Figure 3(b) shows the resulting potential for various doping levels. We obtain a rotation angle for zero doping of $\varphi_0 = 6.3°$. With increasing ρ, we find both a deepening of the potential and, importantly, an increasing displacement of the potential minimum from φ_0. The latter yields a driving force towards an increased AFD rotation which can explain the increase of SL diffraction intensity during the initial time window [Fig. 1(c)]. An increased excess energy of the doped carriers, implemented via an elevated electronic temperature, is predicted to further enhance the effect (Fig. S5). This trend agrees with our experimental observation that fewer *e-h* pairs are needed to generate equivalent enhancements at higher excitation frequencies, e.g., 0.11 *e-h* pairs per f.u. generated by 3.1 eV pump photons yield a similar enhancement as 0.23 *e-h* pairs per f.u. injected by 1.55 eV photons [Fig. 1(c), blue and red data points].

In principle, deepening of the soft-mode potential with constant φ could also enhance the reflection intensity by reducing the average incoherent thermal displacements of the local rotations. This would increase the Debye-Waller factor (DWF) and consequently the reflection efficiency. For our experimental conditions, we expect an initial DWF of >0.99 for the $(\frac{5}{2}\frac{3}{2}\frac{1}{2})$ SL reflection based on the thermal displacement parameters of $EuTiO_3$ [29]. This rules out an increase of I_{AFD} by more than 1% from changes in the DWF. Furthermore, the scaling of the DWF with the x-ray momentum transfer **q** implies that the reflection efficiency would be more strongly enhanced at larger **q**, which is not observed (SM Fig. S2 [25]). Both arguments exclude a significant influence of photoinduced deepening of the double-well potential on the observed dynamics of I_{AFD}.

While the observed photoinduced increase of the OP is contrary to its evolution for increasing temperature (and phonon entropy) in thermal equilibrium, it does not, however, imply an actual decrease of phonon entropy. The increase

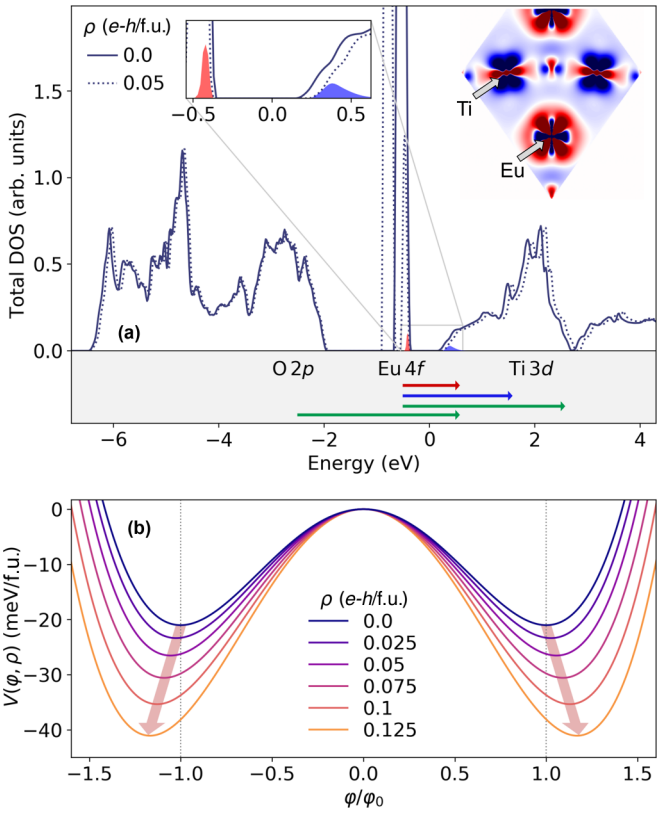

FIG. 3. (a) Calculated $EuTiO_3$ total density of states (DOS) in equilibrium and for an *e-h* concentration of 0.05 *e-h*/f.u. (dotted line). Zero is set to the bottom of the conduction band. Arrows indicate the charge-transfer excitations for photon energies of 1.55 eV (red), 3.1 eV (blue), 4.65 eV (green.) Right inset: Slice in the (101) plane of the *e-h* induced total e^- density difference (blue/red: increase/decrease of electron density). Left inset: Zoom of the DOS in the vicinity of the Fermi level. The solid areas show the density of doped holes (red) and electrons (blue). (b) Double-well potential of the AFD soft mode calculated for a series of *e-h* concentrations ρ.

of φ can be understood intuitively in terms of a reduction of the Goldschmidt tolerance factor [30]: The very general Goldschmidt tolerance factor captures the stability of the perovskite structure in terms of the relative sizes of the *A*- and *B*-site cations. Small tolerance factors, originating from small relative *A*-site cation sizes, are associated with rotations of the (oxygen) octahedra. In contrast, large tolerance factors, indicating large *A*-site cation sizes, favor ferroelectricity through off-centering of the *B*-site cation.

Photoexcitation across the Eu $4f$-Ti $3d$ charge-transfer gap of $EuTiO_3$ [indicated by the top three arrows at the bottom of Fig. 3(a)] removes f electrons from the Eu^{2+} *A*-site ions and shrinks the surrounding electron clouds. Analogously, the Ti^{4+} *B*-site ions expand due to their additional electronic charge. Both size effects decrease the tolerance factor, which is known to cause a more distorted perovskite structure in the static case. We illustrate this in Fig. 3(a), right inset, the calculated change in charge density in the (101) plane (cubic notation). We see that the electron density decreases approximately spherically at the Eu sites and increases at the Ti sites. This unusual decrease in electron density on the Eu^{2+} ion on photodoping is the origin of the stark contrast

in behavior between $EuTiO_3$ and $SrTiO_3$ on photoexcitation, in spite of their equivalent crystallographic structures and O $2p$-Ti $3d$ electronic bands [23,31]. In the case of $EuTiO_3$, the largely unhybridized Eu $4f$ states form an additional set of occupied bands above the oxygen $2p$ valence band; these localized $4f$ states are electron depleted by charge-transfer excitation reducing the size of the Eu^{2+} cation. In contrast, charge-transfer excitation across the O $2p$-Ti $3d$ band gap of $SrTiO_3$ *reduces* the octahedral distortion [9].

Following the excitation, both phonon-mediated *e-h* recombination and cooling of the electronic system via electron-phonon scattering reduce the electronically driven enhancement of φ and heat the phonon system. A rapidly increased temperature of the vibrational system can be expected to further relax the distortion via anharmonic phonon-phonon interactions, similar to a thermally driven phase transition.

All-optical experiments on a $EuTiO_3$ film [25] show a decay dynamics of the photoinduced reflectivity change for 1.55 eV probe photons that resembles a bimolecular decay dynamics. Similar dynamics is observed when probed in the multi-THz regime. We ascribe this decay to an excitation-dependent carrier recombination process (SM [25]).

To model the dynamics of chemical potential φ, we introduce a time dependency of chemical potential $V(\varphi, \rho)$ via a transient doping level $\rho(t)$. The onset dynamics of $\rho(t)$ reflects the pump pulse duration and injected number of *e-h* pairs and the decay dynamics accounts for the recombination process (SM [25]). The temperature increase of the lattice is included via an additional relaxation of $V(\varphi, \rho)$ towards the high-temperature phase along its dependency on ρ. We scale this additional component phenomenologically with the amount of recombined charge carriers at time t (SM [25]). Solving the equation of motion for a time-dependent potential $V(\varphi(t), \rho(t))$ yields $\varphi(t)$ [9], which we numerically fit via $\varphi(t)^2/\varphi_0(t)^2$ to the experimental data [solid lines, Fig. 1(c) (red and blue curves), and Fig. 2].

The model reproduces the slowdown of the decay dynamics for lowering the excitation fluence. As the slowdown is described by an *e-h* density-dependent carrier recombination, we conclude that the lifetime of the enhanced octahedral rotation is mainly governed by the lifetime of the photoinjected carriers. The weak oscillatory component on the decay dynamics of I_{AFD} [Fig. 1(c), red and blue curves] is well reproduced by a model consisting of a displacive excitation caused by a shift of the potential minimum, with the correct phase and frequency, and thus further supports a displacively driven structural dynamics initiated by the optical excitation. The damping of the soft mode is fixed to yield a coherence lifetime of 0.14 ps. The absence of an oscillation after excitation with the shortest wavelength (4.65 eV) photons is possibly related to a delayed buildup of the displacive force due to the opposite effects of the simultaneous O$2p$-Ti$3d$ and Eu$4f$-Ti$3d$ charge-transfer excitations.

We expect that related exotic physics, such as the promotion of ferroelectricity (which is usually associated with lowering temperature) on excitation might occur in certain Mott insulators. For example, in $LaTiO_3$, the top of the valence band is formed from Ti $3d$ states, with the empty La $4f$ states lying about 3–4 eV above the band gap. Excitation between these energy levels will move the Ti valence state towards d^0 occupancy and at the same time cause the size of the *B*-site Ti ion to decrease, and that of the *A*-site La ion to increase, thus increasing the tolerance factor. Both of these effects tend [32] to favor ferroelectricity.

In summary, our ultrafast x-ray diffraction experiments on photoexcited $EuTiO_3$ find a transient increase of the octahedral rotation, opposite to what is expected from an increase of temperature and opposite to what has been observed on isostructural $SrTiO_3$. Such an ultrafast control of a structural distortion in the opposite direction to its thermal transition by optical excitation opens up new possibilities for ultrafast tuning of electronic and magnetic properties [33–35]. In particular, the ability to tune rotations of oxygen octahedra, allows in turn the tuning of magnetic and electronic properties that are strongly correlated with the tolerance factor and structural distortions, such as magnetic orderings or electric polarization, on ultrafast timescales.

We thank H. Lemke for support in processing data acquired at LCLS. Static x-ray characterization of the sample was performed at the X04SA beamline (SLS) with technical assistance from D. Meister. We thank J. L. Mardegan, J. Raab, and M. Furthmeier for technical assistance on the all-optical studies. The research leading to these results has received funding from the Swiss National Science Foundation and its National Centers of Competence in Research, NCCR MUST and NCCR MARVEL. E.M.B. acknowledges funding from the European Community's Seventh Framework Programme (FP7/2007-2013) under Grant Agreement No. 290605 (PSI-FELLOW/COFUND). Computing resources were provided by the MERLIN cluster at the Paul Scherrer Institute. Use of the Linac Coherent Light Source (LCLS), SLAC National Accelerator Laboratory, is supported by the U.S. Department of Energy, Office of Science, Office of Basic Energy Sciences under Contract No. DE-AC02-76SF00515.

[1] E. Morosan, D. Natelson, A. H. Nevidomskyy, and Q. Si, Adv. Mater. **24**, 4896 (2012).

[2] M. Buzzi, M. Först, R. Mankowsky, and A. Cavalleri, Nat. Rev. Mater. **3**, 299 (2018).

[3] M. Eichberger, H. Schafer, M. Krumova, M. Beyer, J. Demsar, H. Berger, G. Moriena, and G. Sciaini, Nature (London) **468**, 799 (2010).

[4] B. Koopmans, G. Malinowski, F. D. Longa, D. Steiauf, M. Fähnle, T. Roth, M. Cinchetti, and M. Aeschlimann, Nat. Mater. **9**, 259 (2010).

[5] T. Rohwer, S. Hellmann, M. Wiesenmayer, C. Sohrt, A. Stange, B. Slomski, A. Carr, Y. Liu, L. M. Avila, M. Kallane, S. Mathias, L. Kipp, K. Rossnagel, and M. Bauer, Nature (London) **471**, 490 (2011).

[6] M. Porer, U. Leierseder, J.-M. Ménard, H. Dachraoui, L. Mouchliadis, I. E. Perakis, U. Heinzmann, J. Demsar, K. Rossnagel, and R. Huber, Nat. Mater. **13**, 857 (2014).

[7] P. Beaud, A. Caviezel, S. O. Mariager, L. Rettig, G. Ingold, C. Dornes, S.-W. Huang, J. A. Johnson, M. Radovic, T. Huber,

T. Kubacka, A. Ferrer, H. T. Lemke, M. Chollet, D. Zhu, J. M. Glownia, M. Sikorski, A. Robert, H. Wadati, M. Nakamura, M. Kawasaki, Y. Tokura, S. L. Johnson, and U. Staub, Nat. Mater. **13**, 923 (2014).

[8] V. Esposito, M. Fechner, R. Mankowsky, H. Lemke, M. Chollet, J. M. Glownia, M. Nakamura, M. Kawasaki, Y. Tokura, U. Staub, P. Beaud, and M. Först, Phys. Rev. Lett. **118**, 247601 (2017).

[9] M. Porer, M. Fechner, E. M. Bothschafter, L. Rettig, M. Savoini, V. Esposito, J. Rittmann, M. Kubli, M. J. Neugebauer, E. Abreu, T. Kubacka, T. Huber, G. Lantz, S. Parchenko, S. Grübel, A. Paarmann, J. Noack, P. Beaud, G. Ingold, U. Aschauer, S. L. Johnson, and U. Staub, Phys. Rev. Lett. **121**, 055701 (2018).

[10] D. Fausti, R. I. Tobey, N. Dean, S. Kaiser, A. Dienst, M. C. Hoffmann, S. Pyon, T. Takayama, H. Takagi, and A. Cavalleri, Science **331**, 189 (2011).

[11] M. Mitrano, A. Cantaluppi, D. Nicoletti, S. Kaiser, A. Perucchi, S. Lupi, P. D. Pietro, D. Pon-tiroli, M. Riccò, S. R. Clark, D. Jaksch, and A. Cavalleri, Nature (London) **530**, 461 (2016).

[12] T. Li, A. Patz, L. Mouchliadis, J. Yan, T. A. Lograsso, I. E. Perakis, and J. Wang, Nature (London) **496**, 69 (2013).

[13] A. Singer, S. K. K. Patel, R. Kukreja, V. Uhlíř, J. Wingert, S. Festersen, D. Zhu, J. M. Glownia, H. T. Lemke, S. Nelson, M. Kozina, K. Rossnagel, M. Bauer, B. M. Murphy, O. M. Magnussen, E. E. Fullerton, and O. G. Shpyrko, Phys. Rev. Lett. **117**, 056401 (2016).

[14] K. W. Kim, A. Pashkin, H. Schäfer, M. Beyer, M. Porer, T. Wolf, C. Bernhard, J. Demsar, R. Huber, and A. Leitenstorfer, Nat. Mater. **11**, 497 (2012).

[15] R. Mankowsky, A. Subedi, M. Först, S. O. Mariager, M. Chollet, H. T. Lemke, J. S. Robinson, J. M. Glownia, M. P. Minitti, A. Frano, M. Fechner, N. A. Spaldin, T. Loew, B. Keimer, A. Georges, and A. Cavalleri, Nature (London) **516**, 71 (2014).

[16] A. Subedi, A. Cavalleri, and A. Georges, Phys. Rev. B **89**, 220301(R) (2014).

[17] R. Mankowsky, M. Fechner, M. Förstt, A. von Hoegen, J. Porras, T. Loew, G. L. Dakovski, M. Seaberg, S. Möller, G. Coslovich, B. Keimer, S. S. Dhesi, and A. Cavalleri, Struct. Dyn. **4**, 044007 (2017).

[18] M. Kozina, M. Fechner, P. Marsik, T. van Driel, J. M. Glownia, C. Bernhard, M. Radovic, D. Zhu, S. Bonetti, U. Staub, and M. C. Hoffmann, Nat. Phys. **15**, 387 (2019).

[19] R. Cowley, Adv. Phys. **29**, 1 (1980).

[20] M. T. Dove, Am. Mineral. **82**, 213 (1997).

[21] D. S. Ellis, H. Uchiyama, S. Tsutsui, K. Sugimoto, K. Kato, D. Ishikawa, and A. Q. R. Baron, Phys. Rev. B **86**, 220301(R) (2012).

[22] V. Goian, S. Kamba, O. Pacherová, J. Drahokoupil, L. Palatinus, M. Dušek, J. Rohlíček, M. Savinov, F. Laufek, W. Schranz, A. Fuith, M. Kachlík, K. Maca, A. Shkabko, L. Sagarna, A. Weidenkaff, and A. A. Belik, Phys. Rev. B **86**, 054112 (2012).

[23] J. L. Bettis, M.-H. Whangbo, J. Köhler, A. Bussmann-Holder, and A. R. Bishop, Phys. Rev. B **84**, 184114 (2011).

[24] J. H. Lee, X. Ke, N. J. Podraza, L. F. Kourkoutis, T. Heeg, M. Roeckerath, J. W. Freeland, C. J. Fennie, J. Schubert, D. A. Muller, P. Schiffer, and D. G. Schlom, Appl. Phys. Lett. **94**, 212509 (2009).

[25] See Supplemental Material at http://link.aps.org/supplemental/10.1103/PhysRevResearch.1.012005 for additional information on experimental details, characterization of the sample, all-optical experiments and details about the theoretical descriptions and the models used.

[26] P. J. Ryan, J.-W. Kim, T. Birol, P. Thompson, J.-H. Lee, X. Ke, P. S. Normile, E. Karapetrova, P. Schiffer, S. D. Brown, C. J. Fennie, and D. G. Schlom, Nat. Commun. **4**, 1334 (2013).

[27] L. A. A. Pettersson, L. S. Roman, and O. Inganäs, J. Appl. Phys. **86**, 487 (1999).

[28] The ELK LAPW code, http://elk.sourceforge.net.

[29] M. Allieta, M. Scavini, L. J. Spalek, V. Scagnoli, H. C. Walker, C. Panagopoulos, S. S. Saxena, T. Katsufuji, and C. Mazzoli, Phys. Rev. B **85**, 184107 (2012).

[30] V. M. Goldschmidt, Naturwissenschaften **14**, 477 (1926).

[31] T. Birol and C. J. Fennie, Phys. Rev. B **88**, 094103 (2013).

[32] N. A. Benedek and C. J. Fennie, J. Phys. Chem. C **117**, 13339 (2013).

[33] M. Imada, A. Fujimori, and Y. Tokura, Rev. Mod. Phys. **70**, 1039 (1998).

[34] B. B. V. Aken, T. T. M. Palstra, A. Filippetti, and N. A. Spaldin, Nat. Mater. **3**, 164 (2004).

[35] J. Varignon, M. N. Grisolia, J. Íñiguez, A. Barthélémy, and M. Bibes, npj Quantum Mater. **2**, 21 (2017).